Determination of Conformational Entropy of Fully and Partially Folded Conformations of Holo-and Apomyoglobin

ARTICLE *in* THE JOURNAL OF PHYSICAL CHEMISTRY B · JANUARY 2015

Impact Factor: 3.3 · DOI: 10.1021/jp509732q

3 AUTHORS, INCLUDING:

Andreas Stadler
Forschungszentrum Jülich
30 PUBLICATIONS **245** CITATIONS

THE JOURNAL OF PHYSICAL CHEMISTRY B

Article

pubs.acs.org/JPCB

Determination of Conformational Entropy of Fully and Partially Folded Conformations of Holo- and Apomyoglobin

Andreas M. Stadler,*[,†] Michael Marek Koza,[‡] and Jörg Fitter[§,∥]

[†]Jülich Centre for Neutron Science JCNS and Institute for Complex Systems ICS, Forschungszentrum Jülich GmbH, 52425 Jülich, Germany

[‡]Institut Laue-Langevin, CS 20156, 38042 Grenoble, France

[§]Institute of Complex Systems (ICS-5): Molecular Biophysics, Forschungszentrum Jülich GmbH, 52425 Jülich, Germany

[∥]I. Physikalisches Institut (IA), AG Biophysik, RWTH Aachen, Sommerfeldstrasse 14, 52074 Aachen, Germany

Supporting Information

ABSTRACT: Holo- and apomyoglobin can be stabilized in native folded, partially folded molten globules (MGs) and denatured states depending on the solvent composition. Although the protein has been studied as a model system in the field of protein folding, little is known about the internal dynamics of the different structural conformations on the picosecond time scale. In a comparative experimental study we investigated the correlation between protein folding and dynamics on the picosecond time scale using incoherent quasielastic neutron scattering (QENS). The measured mean square displacements (MSDs) of conformational motions depend significantly on the secondary structure content of the protein, whereas the correlation times of the observed internal dynamics were found to be similar irrespective of the degree of folding. The conformational entropy difference ΔS_{conf} between the folded conformations and the acid denatured state could be determined from the measured MSDs and was compared to the entropy difference ΔS obtained from thermodynamic parameters reported in the literature. The observed difference between ΔS and ΔS_{conf} was attributed to the entropy difference ΔS_{hydr} of dynamically disordered water molecules of the hydration shell. The entropy content of the hydration water is significantly larger in the native folded proteins than in the partially folded MGs. We demonstrate the potential of incoherent neutron scattering for the investigation of the role of conformational dynamics in protein folding.

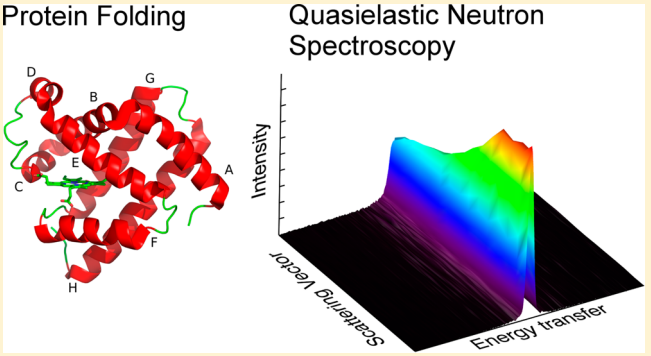

1. INTRODUCTION

The central process in protein folding is the collapse of the unfolded polypeptide chain into a compact globular conformation, the formation of secondary structure elements, and finally the creation of the fully folded protein structure. Apomyoglobin (apo-Mb), myoglobin without the heme group, serves as a model system in the field of protein folding, as fully folded conformations, partially folded states, and disordered chains can be stabilized under equilibrium conditions.[1−3] Partially folded equilibrium configurations of apo-Mb are believed to mimic kinetic intermediates along the folding pathway.[4−6] The partially folded conformations of apo-Mb are considered as molten globules (MGs), which have a compact shape, a certain population of folded secondary structure elements, but lack the complete specific side chain interactions, which are present in the folded structure.[7]

The underlying physical principle, which governs the folding process of a protein from a disordered and unstructured configuration to a folded conformation, is the thermodynamic difference of the free energy ΔG between the unfolded and the folded state ($\Delta G = \Delta G_{unfolded} - \Delta G_{folded} = \Delta H - T \times \Delta S$). Major components of the enthalpic stabilization ΔH in proteins are weak van der Waals forces, hydrogen bonds, and, to a smaller extent, screened electrostatic interactions.[8] Protein conformational entropy and disordered water molecules in the hydration shell account for the entropic contribution $T \times \Delta S$ and play an important role during the folding process. However, the interplay of both entropic components is complex: In the unfolded state a protein is generally more flexible than in a folded conformation, which leads to an entropic stabilization of the unfolded state as compared to the folded conformation. On the other hand, buried hydrophobic residues from the core of the protein are exposed to the solvent in the unfolded state, which strongly modifies the properties of the hydration shell. The interaction of the hydrophobic residues with hydration water leads to a more ordered water structure

Received: September 25, 2014
Revised: December 11, 2014

   dx.doi.org/10.1021/jp509732q | J. Phys. Chem. B XXXX, XXX, XXX−XXX

around these amino acids,[9] which reduces the entropy content of the unfolded state and stabilizes the folded conformation.

The sampling of different structural conformations is responsible for the conformational entropy of the protein. Classical thermodynamic methods always detect the combined entropy components of both the protein and the hydration water, whereas neutron spectroscopy allows the direct measurement of conformational motions in proteins on the picosecond to nanosecond time scale.[10] Average conformational fluctuations in proteins are probed by incoherent neutron scattering, as the incoherent scattering cross section of protons is the largest of all elements occurring in biological macromolecules, and hydrogen atoms are uniformly distributed in proteins. Quasielastic incoherent neutron scattering (QENS) provides spatiotemporal information on internal diffusive motions in proteins, as both scattering vector (q) and energy resolved spectra are recorded. Picosecond dynamics in proteins measured by QENS have been interpreted to arise predominately from amino acid side chain rotations and librations[11] and therefore inform about side chain rotamer transitions.[12] Thus, QENS measurements covering the picosecond time scale are a direct method to quantify the contribution of side chain dynamics to protein conformational entropy.[13]

In this article we report on a comparative study of picosecond dynamics of native folded, partially folded, and unfolded conformations of holo- and apo-Mb measured by neutron time-of-flight spectroscopy. The measured MSDs allowed the determination of the conformational entropy of the different conformations with respect to the acid denatured state. The obtained entropy differences from neutron scattering could be compared to thermodynamic results from the literature, which allowed the disentanglement of protein and hydration layer components.

2. MATERIAL AND METHODS

2.1. Sample Preparation. Horse heart Mb (Sigma-Aldrich, St. Louis, MO) was dissolved in distilled water. The pH was then lowered to 1.5 with concentrated HCl, and the solution was mixed with 4 volumes of 2-butanone. The upper organic layer was decanted, and the process was repeated until the heme extraction was complete. The obtained apo-Mb solution was extensively dialyzed against buffer (20 mM NaH_2PO_4/Na_2HPO_4 pH 7) followed by distilled water. The apo-Mb solution was then lyophilized. Freeze-dried apo-Mb and holo-Mb powders were dissolved in heavy water (99.9 atom % D, Sigma-Aldrich) to remove the exchangeable protons, incubated for 1 day, and lyophilized again. The D_2O exchanged powder samples were dissolved in the different D_2O buffers (20 mM NaH_2PO_4/Na_2HPO_4 for both buffers at pD 4 and 6; 10 mM DCl for the buffer at pD 2; 10 mM DCl, 20 mM NaTCA at pD 2; 10 mM DCl, 100 mM NaCl at pD 2) at a concentration of approximately 5 mg/mL and dialyzed against the corresponding buffer in 100 excess volume (Slide-A-Lyzer dialysis devices, 3,500 MWCO, Thermo Scientific, Rockford, IL). The buffer exchanged protein solutions were concentrated to the final concentrations (Vivaspin 3,000 MWCO concentration units, Sartorius, Goettingen, Germany). The pD was calculated by adding 0.4 to the value measured on a normally calibrated pH meter.[14] Deuterated DCl (99 atom %, Sigma-Aldrich) was used for pD adjustment of the D_2O buffers. Protein concentration was measured using UV/vis absorption spectroscopy (NanoDrop 2000c, Thermo Scientific). The concentration of the apo-Mb solutions was determined with the calculated extinction coefficient of $E_{1\%}$ = 8.25 at 280 nm from the amino acid sequence using the ExPASy Web server.[15] Holo-Mb was found to be in the oxygenated state, and the concentration was determined with the extinction coefficients of 13.9 and 14.4 mM^{-1} cm^{-1} at 542 and 579 nm, respectively, and the molecular mass of 18.8 kDa as reported by Antonini and Brunori.[16] The final concentrations were close to 50 mg/mL with the exception of apo-Mb at pD 2 with 0.1 M NaCl and apo-Mb at pD 6, which had concentrations of 40 and 100 mg/mL, respectively. The highly concentrated protein solutions of the unfolded and partially folded conformations had a high viscosity, but did not show any precipitation.

2.2. QENS Experiments. The neutron scattering experiments were performed on the cold neutron time-of-flight spectrometer IN6 at the ILL (Grenoble, France).[17] The incident wavelength was set to 5.1 Å, which resulted in an energy resolution of around 100 μeV (fwhm). The instrumental resolution function was determined by a vanadium measurement. The protein solutions including all buffers were measured at a temperature of 16 °C for at least 4 h per sample. The flat sample holders were oriented at 135° with respect to the incident neutron beam direction. The measured spectra were corrected for energy dependent detector efficiency, normalized to vanadium, and transformed into energy transfer and scattering vector space. Data reduction was done with the software package LAMP.[18] Data were binned into groups of Δq = 0.1 $Å^{-1}$. The concentrated protein solutions and the corresponding buffers, each around 1.5 mL, were measured in flat aluminum sample holders with a thickness of 1 mm. The sample holders were sealed with indium wire against vacuum. By weighing the sealed samples before and after the neutron measurements it was verified that no loss of material occurred during the experiments.

The signal from the D_2O buffers was weighted by the transmission factors $f = T_{protein}/T_{buffer}$ and subtracted from the intensities of the protein solutions, where $T_{protein}$ and T_{buffer} are the measured transmissions of the protein solution and the corresponding D_2O buffer, respectively.

2.3. Small-Angle Scattering. Small-angle scattering by neutrons and X-rays (SANS and SAXS) was measured for different samples. An extensive description of the small-angle scattering technique applied to the study of biological macromolecules can be found in the review of Svergun and Koch.[19] Transmissions of the concentrated apo-Mb samples with a 1 mm thickness were measured on the small-angle diffractometer D22[17] at the ILL using a neutron wavelength of 6 Å, which is close to the wavelength of the neutron spectroscopy experiments. The transmission of holo-Mb was not measured, but the corresponding value of apo-Mb was taken. The collimation and the sample-to-detector distances were 11.2 m. Transmission factors f used for the correction of the QENS data were found to lie between 0.95 and 0.98 for the measured protein solutions and buffers.

SAXS was measured for the proteins on the beamline BM29[20] at the ESRF (Grenoble, France). Protein concentrations were between 1.4 and 50 mg/mL. The samples were measured in D_2O buffers at a temperature of 8 °C. The Guinier radius was determined using the indirect Fourier transform method implemented in the GNOM package in the limit of infinite dilution.[21]

2.4. Circular Dichroism and Dynamic Light Scattering. Circular dichroism (CD) was measured to estimate the protein secondary structure. A J-810 spectropolarimeter (JASCO,

dx.doi.org/10.1021/jp509732q | J. Phys. Chem. B XXXX, XXX, XXX−XXX

Tokyo, Japan) was used for the measurements. The protein solutions were measured at a concentration of approximately 0.5 mg/mL in 1 mm-thick quartz cuvettes under constant nitrogen flow in a wavelength range from 180 to 280 nm at 20 °C. The secondary structure content was estimated using the deconvolution algorithms available within the CDPro software package.[22]

Dynamic light scattering (DLS) was measured on a Zetasizer Nano ZS instrument (Malvern Instruments, Malvern, United Kingdom) at 20 °C at concentrations between 1.3 and 50 mg/mL. The autocorrelation functions were analyzed using the CONTIN algorithm.[23] The hydrodynamic radius R_h was determined according to $R_h = k_B T/(6\pi\eta D)$ with the viscosities of D_2O η = 1.251 cP and of 8 M Urea in D_2O η = 1.910 cP at 20 °C.

2.5. QENS Data Analysis. A detailed description of the QENS technique can be found in the book of Bée.[24] A more specific review regarding the application of QENS for biomolecular dynamics can be found in the book edited by Fitter, Gutberlet, and Katsaras.[10] In general, the theoretical incoherent quasielastic scattering function $S(q, \omega)$ due to diffusive molecular motions in soft condensed matter and biological systems can be written as[10]

$$S(q, \omega) = A_0(q) \times \delta(\omega) + \sum_{n=1}^{N} A_n(q) \times L_n(q, \omega) \quad (1)$$

where $A_0(q)$ is the elastic incoherent structure factor (EISF), which contains the relevant information about the geometry of molecular motions that are confined with respect to the length−time window of the neutron spectrometer. The L_n are Lorentzians, which describe the quasielastic broadening of their number N depending on the specific model.

In the simplest model, the QENS spectra can be interpreted according to

$$S(q, \omega) = A_0(q) \times \delta(\omega) + (1 - A_0(q)) \times L(q, \omega) \quad (2)$$

where one effective Lorentzian is fitted to the quasielastic broadening. The Lorentzian has the form

$$L(q, \omega) = \frac{1}{\pi} \cdot \frac{\Gamma(q)}{(\hbar\omega)^2 + \Gamma(q)^2} \quad (3)$$

where $\Gamma(q)$ is the half-width at half-maximum. The scattering function $S(q, \omega)$ plus linear background $B(\omega)$ was convoluted with the instrumental resolution function $S_{res}(q, \omega)$ and fitted to each measured spectra $S(q, \omega)_{meas}$ according to

$$S_{meas}(q, \omega) = [\exp(-\langle x_{vib}^2 \rangle q^2) \times S(q, \omega) + B(\omega)] \otimes S_{res}(q, \omega) \quad (4)$$

MSDs of fast vibrational motions $\langle x_{vib}^2 \rangle$ were taken into account by a Debye−Waller factor. The fits were performed over the energy transfer range from −1.5 meV to +1.5 meV. Each instrumental resolution function $S_{res}(q, \omega)$ was determined by measuring a vanadium standard sample.

3. RESULTS AND DISCUSSION

3.1. Structural Characteristics and Thermodynamic Properties. Mb serve as well-suited and classical model systems in the field of protein folding[1] and protein dynamics.[25] The native form of Mb carries one heme group, which can bind reversibly one oxygen molecule. The heme-bound Mb is called "holo-Mb" in the literature with the word "holo" stemming from ancient Greek, which means "whole" or "complete". The structure of holo-Mb has been solved by X-ray crystallography[26] and is shown in Figure 1.

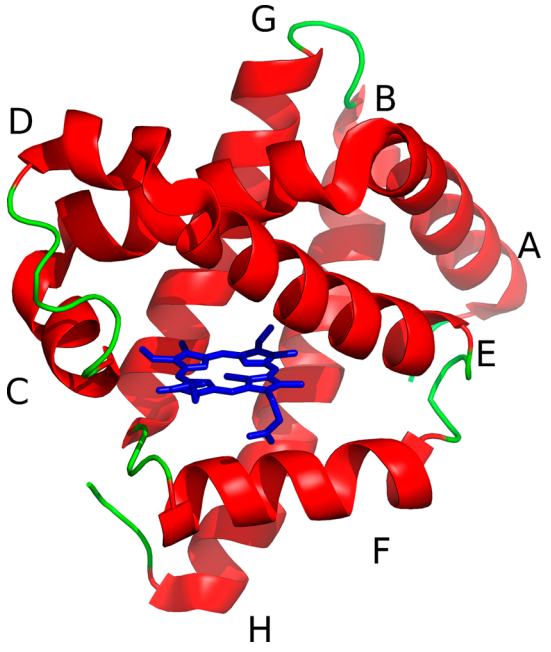

Figure 1. Structure of myoglobin (pdb code 2V1K). Letters label the helices. Helices and loop regions are drawn in red and green. The heme group is drawn with solid lines in blue.

The native Mb protein consists of 153 amino acids, which are arranged in eight α-helices labeled from A to H with connecting loops. The heme group is embedded into a pocket formed between helices E and F. The removal of the heme group destabilizes the protein, and the heme-free protein—the so-called apo-Mb—can be trapped in different partially folded and unfolded conformations depending on the solvent condition. The word "apo" comes from ancient Greek meaning "without", which refers to the heme-free state. The standard terminology concerning the structure of the partially folded states also refers to the α-helices of the holo-protein even though not all helices are fully formed in the unfolded conformations. The partially folded structures could not be crystallized yet, but valuable structural information was obtained by using NMR spectroscopy.[4,27−30] The majority of native apo-Mb at pH 6 adopts a well-defined structure, which is very similar to that of holo-Mb.[27] The E-F loop, the F helix, the F-G loop, and the beginning of the G-helix are unstructured due to conformational fluctuations and disorder.[27] One MG conformation, the so-called I1 state, of apo-Mb can be stabilized at pH 4 at low salt,[5] whereas a second MG state I2, which contains a larger amount of secondary structure content, can be stabilized by the trichloracetate (TCA) anion either from the acid denatured state or from the I1 state.[4] The I1 and I2 states are considered to be similar to transient folding intermediates, which lie on the folding pathway of apo-Mb.[6] A model of the MG of apo-Mb at pH 4 was suggested,[28,29] which consists mainly of the folded hydrophobic nucleus formed by the helices A, G, and H. In the MG I2 state the helical core region AGH becomes more stabilized and the B helix folds additionally on top of the AGH nucleus, thus increasing the secondary structure content.[4] A

dx.doi.org/10.1021/jp509732q | J. Phys. Chem. B XXXX, XXX, XXX−XXX

Table 1. Secondary Structure Content and Thermodynamic Parameters of the Different Conformational States of apo-Mb and holo-Mb Investigated by QENS[a]

protein	state	α-helical content* (%)	α-helical content† (%)	T_m (°C)	ΔH (kJ/mol/K)	ΔC_p (kJ/mol)
apo-Mb at pH 2	unfolded	6	5	–	–	–
apo-Mb at pH 2, 100 mM NaCl	MG	22	28	60	63.3	0.82
apo-Mb at pH 4	MG I1	43	35	–	–	–
apo-Mb pH 2, 20 mM NaTCA	MG I2	49	45	60	72.5	0.69
apo-Mb at pH 6	folded	54	55	61	222	6.5
holo-Mb pH 6	folded	66	66	81	615	11.9

[a]The α-helical content* was measured by CD. The thermodynamic parameters ΔH, ΔC_p, and the α- helical content† are compiled from the literature.[5,31,33−35] T_m is the midpoint denaturation temperature calculated from ΔH and ΔC_p, where the folded and unfolded states are equally populated.

third partially folded conformation of apo-Mb with less secondary structure content can be stabilized from the acid denatured state by the chloride anion,[31,32] but that structural conformation has received less attention in the literature. We consider the acid denatured state of apo-Mb at pH 2 in this article as a reference for the unfolded state. The acid denatured state, however, is not fully unfolded. Residual helical structure elements were found in helices A and H, and local hydrophobic clusters, in helices B and G.[30] The small amount of stabile helical structure found by circular dichroism (see Table 1) agrees quantitatively with the most stabile helical core region of helix H (residues 132−141) found by NMR.[30]

The secondary structure content of the different samples investigated by QENS was determined using CD. The measured CD spectra are shown in Figure 2. The estimated

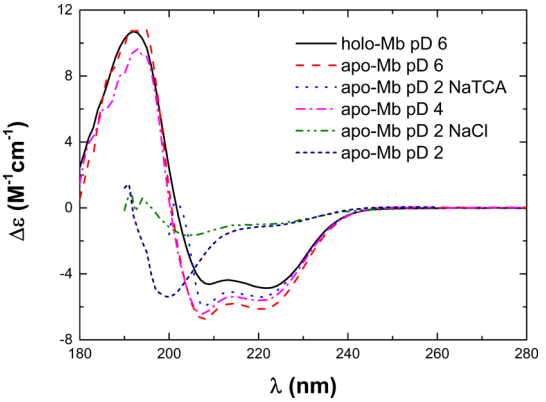

Figure 2. Measured CD spectra of the different conformational states of apo- and holo-Mb.

secondary structure content of the proteins in the different solvent conditions from the CD measurement and the known literature values are summarized in Table 1. The measured α-helical content of the samples is in agreement with the reported literature values. The α-helical content of apo-Mb at pD 4 was found to be larger than the reported literature value, but the deviation is within the accuracy of the secondary structure estimation of around 5−10% by CD.

The secondary structure content of the partially folded and unfolded proteins might be increased in the concentrated 5% solutions used for the neutron scattering experiments due to macromolecular crowding. However, a SANS study showed that macromolecular crowding does not induce folding of an intrinsically disordered protein (N protein of bacteriophage λ) even at a very high crowder concentration of 130 mg/mL.[36] Single-molecule FRET experiments on different intrinsically disordered proteins revealed only small changes of a few percent of the R_G at polymer crowder concentrations of 5%.[37] Macromolecular crowding also did not have any significant effects on the refolding of acid denatured lysozyme[38] or urea denatured ribonuclease A[39] up to crowder concentrations of 10%. Therefore, macromolecular crowding probably has a minor effect on protein refolding in the 5% protein solutions measured by QENS in our study. Furthermore, the protein concentration of 50 mg/mL is far below the critical overlap concentration of $c^* = M/[(4\pi/3)R_G^3 N_A] = 245$ mg/mL, where we take the largest $R_G = 3.02$ nm of the acid unfolded apo-Mb.

The different conformational states were characterized by DLS and by SAXS. The MGs might be sensitive to the oligomeric state. Volume fractions of the monomeric protein between 99% and 100% were found for the 5% solutions by DLS. DLS clearly shows the absence of larger oligomers, but the method does not allow distinguishing reliably between monomers and small oligomers, e.g. dimers. SAXS was measured for the concentrated 5% solutions and diluted aliquots directly before the QENS experiments. The measured SAXS data of the apo-Mb samples (acid denatured, MGs I1 and I2, and the folded state) are shown in Figure 3. The molecular mass was determined from the extrapolated forward scattering

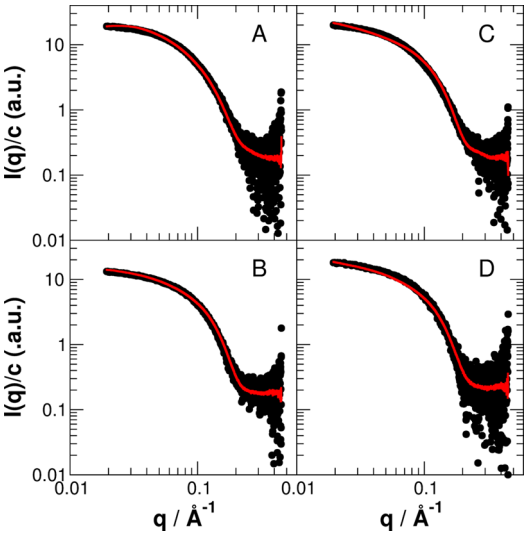

Figure 3. Measured SAXS data of (A) the acid denatured apo-Mb, (B) the MG I1 state, (C) the MG I2 conformation, and (D) the folded conformation of apo-Mb. The black circles correspond to measured data of diluted solutions with concentration between 2.3 and 2.8 mg/mL. The red lines give the measured data of the concentrated protein solutions with concentrations close to 50 mg/mL.

dx.doi.org/10.1021/jp509732q | J. Phys. Chem. B XXXX, XXX, XXX−XXX

$I(q \to 0)/c$ of the diluted solutions. The molecular mass was found to lie between 13.3 and 20.0 kDa being in agreement with the calculated molecular mass of 17.0 kDa for the apo-Mb monomer. Small variations of the molecular mass are related to uncertainties of the measured protein concentrations. The plots of $I(q)/c$ of the diluted and the concentrated solutions overlap, which directly confirms that apo-Mb forms monomers in the 5% solutions and that the shape of the protein remains similar from the diluted to the concentrated range. Weak interparticle interactions were found for the 5% apo-Mb solutions, which cause only small modulations of the SAXS curves. The molecular mass determined from the $I(q \to 0)/c$ for the concentrated solutions of the MGs I1 and I2 was found to be 14.0 and 21.0 kDa (dilute solutions: 13.3 and 20.0 kDa), respectively. The slightly larger molecular mass of the concentrated solutions M_{conc} might be caused by a small fraction of dimers or tetramers $M_{conc} = \phi \cdot M_{monomer} + (1 - \phi) \cdot M_X$, where M_X is the molecular mass of the dimer or tetramer. Assuming dimers (or tetramers), we obtain a volume fraction of ϕ = 95% (or 98%) for the monomeric protein for both MGs I1 and I2. Hence, the MGs I1 and I2 are predominantly monomers in the concentrated solutions, and any changes due to oligomerization can be fully neglected.

The 5% solution of the NaCl stabilized MG was found to be very viscous, and DLS or SAXS was not measured. The MG stabilized by NaCl was found to oligomerize even in dilute protein solutions by Kataoka.[32] Therefore, we cannot give any information about the oligomerization state in concentrated solution, and we did not measure the R_h or the R_G of the MG stabilized by NaCl. The hydrodynamic radius R_h and the Guinier radius R_G given in Table 2 were determined from dilute protein solutions. The R_h/R_G ratio allows gaining further information on the compactness of the different conformational states. That information is complementary to the CD measurements, which are informative regarding the local ordered secondary structure. The determined R_h/R_G values are given in Table 2.

Table 2. Hydrodynamic Radii R_h, Guinier Radii R_G, and the Ratio R_h/R_G of Different Unfolded, Partially Folded, and Native States of apo- and holo-Mb[a]

protein	state	R_h (nm)	R_G (nm)	R_h/R_G
apo-Mb 8 M Urea	unfolded	3.33	4.67	0.71
apo-Mb at pD 2	unfolded	2.85	3.44	0.83
apo-Mb at pD 4	MG I1	2.27	1.94	1.17
apo-Mb pD 2, 20 mM NaTCA	MG I2	2.63	2.29	1.15
apo-Mb at pD 6	folded	2.55	1.98	1.29
holo-Mb at pD 6	folded	2.20	1.75	1.26
Myelin Basic Protein	intrinsically disordered	3.57	3.30	1.08

[a]The corresponding literature values of the intrinsically disordered myelin basic protein are also given.[40]

For Gaussian chain polymers in good and θ solution, the R_h/R_G has values of 0.66 and 0.64, respectively. Only the fully denatured state of apo-Mb in 8 M Urea, which has zero secondary structure,[32] approaches that value. The acid denatured state has a larger R_h/R_G value and therefore a higher compactness, which is caused by the residual helical structure elements and the local hydrophobic clusters. The native folded apo- and holo-Mb on the other hand have a large R_h/R_G value and a high compactness being nearly identical to that of a sphere, which has a theoretical R_h/R_G ratio of $(5/3)^{0.5}$ = 1.29. The MGs I1 and I2, however, have intermediate compactness and their R_h/R_G value lie between the unfolded and the folded proteins. The reason is that the folded hydrophobic nucleus AGH increases the compactness of the MGs. The compactness of the MGs I1 and I2 is slightly larger than that of the intrinsically disordered myelin basic protein, which has a similar secondary structure of 44%[40] as the MGs. The reason is probably the lower charge of the MGs compared to the intrinsically disordered protein, which results in a more compact structure.

Folding of a protein from a disordered state into the folded structure is determined by the free energy difference of the macromolecule. The known thermodynamic parameters of the MGs, and the folded states are summarized in Table 1. The free energy difference $\Delta G(T)$ was calculated using the Gibbs–Helmholtz equation

$$\Delta G(T) = \Delta H\left(1 - \frac{T}{T_m}\right) + \Delta C_p\left[T - T_m - T\ln\left(\frac{T}{T_m}\right)\right] \quad (5)$$

and the entropy difference $\Delta S(T)$ according to

$$\Delta S(T) = \frac{\Delta H}{T_m} + \Delta C_p \ln\left(\frac{T}{T_m}\right) \quad (6)$$

The calculated free energy difference ΔG and the entropy difference ΔS of the different conformational states are shown in Figure 4A and B. It is clearly visible that the removal of the heme group changes the free energy and entropy differences strongly compared to the holo-protein. In native apo-Mb the lower value of ΔH reduces the ΔG over the whole temperature range and thus destabilizes the protein. The MGs have a similar melting temperature as the native apo-Mb, although the enthalpy difference ΔH of the MGs is much smaller than that of native apo-Mb. The reason for the similar melting temperature T_m of native apo-Mb and the MGs is the smaller entropy difference ΔS of the MGs, which results in a flatter slope of $\Delta G = \Delta H - T\Delta S$ and shifts the T_m to a higher temperature. At lower temperatures the ΔS of native apo-Mb and holo-Mb become negative, while the entropy difference of the MGs is close to zero (compare Figure 4B). We need to remember here that ΔS consist of two parts: the conformational entropy difference of the protein and the entropy difference of the hydration water. A negative value of ΔS shows that the reduction in entropy due to the more ordered hydration layer around the unfolded protein compensates the gain in conformational entropy of the protein in the unfolded conformation. It is an interesting question how the conformational entropy of the protein differs between the folded and partially folded states of apo- and holo-Mb in such a case. In the following section we present direct measurements of the conformational entropy of the proteins in the picosecond time scale by QENS at a temperature of 16 °C, where the described effect can readily be observed. We have chosen 16 °C, as ΔG has got a comparable value for the different apo-Mb states at that temperature; see Figure 4. We recall that

$$\Delta G(T) = RT\ln(f_F/f_U) \quad (7)$$

with f_F and f_U being the population numbers of the folded and unfolded states, respectively. At a similar value of ΔG the

dx.doi.org/10.1021/jp509732q | J. Phys. Chem. B XXXX, XXX, XXX–XXX

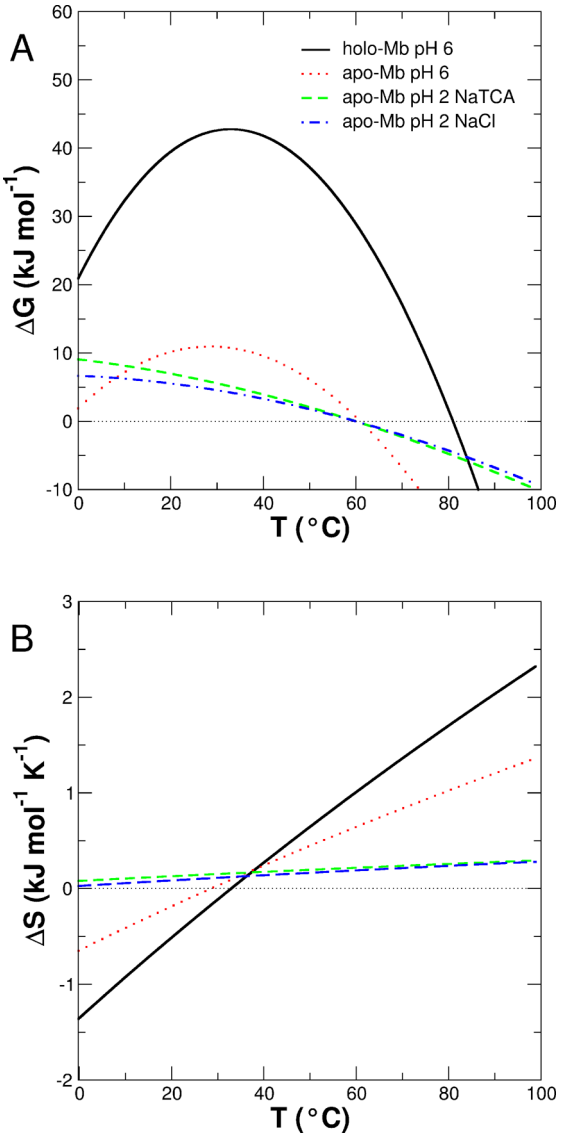

Figure 4. (A) Free energy difference ΔG of the proteins in the folded conformations and the partially folded MGs. (B) Entropy difference ΔS of the different conformations. The temperature dependence of ΔG and ΔS was calculated using the Gibbs−Helmholtz equation with the available thermodynamic parameters reported in Table 1

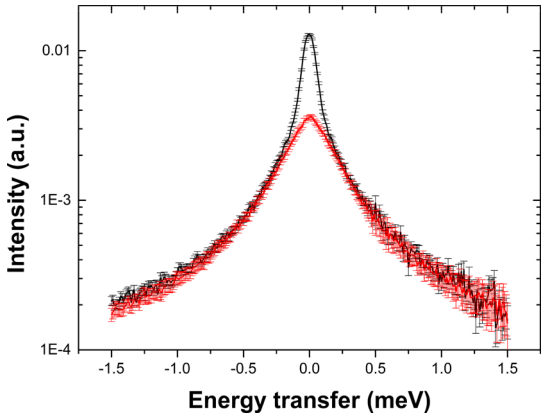

Figure 5. Measured QENS spectra at q = 1.5 Å^{-1} of native apo-Mb at pD 6 before buffer subtraction (black) and D_2O buffer (red).

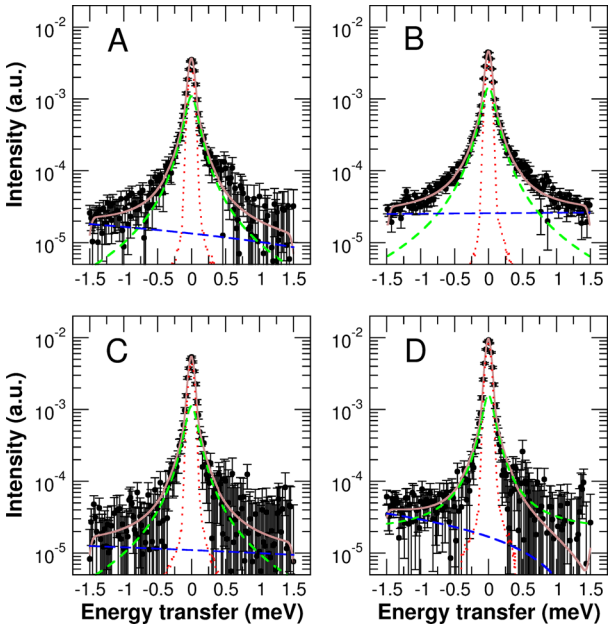

Figure 6. Measured QENS spectra of apo-Mb in different folded states with subtracted D_2O buffer at the scattering vector q = 1.5 Å^{-1}. For more clarity only every second data point is drawn. (A) Acid denatured state of apo-Mb at pH 2, (B) MG of apo-Mb with 100 mM NaCl at pH 2, (C) MG I2 of apo-Mb stabilized with 20 mM NaTCA at pH 2, (D) native state of apo-Mb at pH 6. The circles are measured data, and the solid brown line represents the total fit to the data. The components correspond to the elastic fraction (red dotted line), the Lorentzian (green dashed line), and the linear background (blue dashed-dotted line). The total fits and the components are convoluted with the instrumental resolution function.

populations of folded and unfolded states are therefore similar. At the melting temperatures T_m reported in Table 1 $\Delta G(T_m)$ = 0 with $f_U = f_F$.

3.2. Protein Dynamics Measured by QENS. Conformational fluctuations of the different structural states of apo- and holo-Mb in the picosecond time scale were measured using neutron time-of-flight spectroscopy. A typical QENS spectrum at q = 1.5 Å^{-1} of native apo-Mb before buffer subtraction and the corresponding D_2O buffer is shown in Figure 5.

A strong difference between the protein solution and the buffer emerges for the elastic peak region, but the scattered intensities of the protein solution approach the signal from the buffer in the quasielastic range. Therefore, good counting statistics are needed to obtain reliable information regarding the quasielastic scattering from the protein solution with subtracted buffer contribution. Representative QENS spectra of the protein solutions after buffer subtraction at the scattering vector q = 1.5 Å^{-1} are shown in Figure 6. The spectra summed over the whole detector are shown in Figure S1 in the Supporting Information. The q-dependent spectra could be fitted well using one δ-function plus one Lorentzian for the quasielastic broadening plus linear background. The χ^2 of the fit to the whole data sets of apo-Mb at pD 2, pD 2 with NaTCA, pD 4, and pD 6 lie between 0.65 and 0.90 due to the large error bars. Fitting a more complex model consisting of one δ-function plus two Lorentzians plus linear background yields χ^2 values between 0.66 and 1.02, thus giving equally good or even slightly worse fits. The data of apo-Mb with NaCl and holo-Mb have significantly better statistics. The χ^2 of the fit of the one Lorentzian model to the whole data sets of apo-Mb with NaCl

dx.doi.org/10.1021/jp509732q | J. Phys. Chem. B XXXX, XXX, XXX−XXX

and holo-Mb were 2.12 and 2.30, respectively. By fitting the more complex two Lorentzian model, χ^2 values of 1.79 for apo-Mb with NaCl and 3.16 for holo-Mb are obtained. Increasing the number of free parameters results in a small reduction of the χ^2 value for the data of apo-Mb with NaCl. For holo-Mb the more complex two Lorentzian model even gives a worse fit to the data. Usually the simplest model, which describes the experimental data, is the best choice. To quantify the statistical significance that a model describes the experimental data, several selection criteria exist. The Akaike information criterion (AIC)[41] is one of them defined by $AIC = \chi^2 + 2p + [(2p(p + 1))/(N - p - 1)]$, where p is the number of free parameters and N is the number of data points. The model, which has the smallest AIC, is the most probable description of the experimental data. In our case $p = 6$ for the one Lorentzian model, $p = 8$ for the two Lorentzian model, and $N = 300$ for one spectrum. For the data of apo-Mb NaCl we obtain AIC = 14.4 for the one Lorentzian model and AIC = 18.3 for the two Lorentzian model, or ΔAIC = 3.9. Therefore, although the χ^2 is slightly reduced for apo-Mb with NaCl the two Lorentzian model with ΔAIC = 3.9 is statistically not a better model compared to the one Lorentzian model. In recent work we could describe the complete dynamic structure factor of hydrated hemoglobin in the quasielastic range using the analytical model of the overdamped Brownian oscillator.[12] We found that one effective Lorentzian describes the quasielastic broadening equally well as the theoretical model of the Brownian oscillator. However, counting statistics with high accuracy are needed for the interpretation of the QENS spectra using a full analytical theory, which is unfortunately not the case for the data presented in this work.

The relevant information about diffusive confined protein motions is contained in the scattering vector dependence of the elastic peak and of the half-widths $\Gamma(q)$ of the quasielastic broadening. The EISF was interpreted using the Gaussian approximation according to

$$A_0(q) = A \cdot e^{-\langle x^2 \rangle q^2} \cdot (1 - p) + p \quad (8)$$

where $\langle x^2 \rangle$ is the MSD of the observed diffusive fluctuations and p accounts for a fraction of slow moving hydrogen atoms, which appear as immobile within the energy resolution of the neutron spectrometer. The measured EISFs and the fits using eq 8 are shown in Figure 7. Theoretically, the EISF has to converge toward unity as q approaches zero. The prefactor A needs to be introduced in the model, as the measured EISFs do not intercept unity for $q \to 0$. A small contribution of multiple scattering and absorption due to the large D_2O volume[42,43] is the easiest and by far most likely explanation for the deviation of the EISFs from unity. A more subtle reason for the observed effect could be a displacement distribution with a small contribution of motions with large amplitudes as pointed out by Doster and Settles.[44] Large amplitudes of motion would lead to an additional increase of the EISF at small q-values. For the apo-Mb samples the prefactor was found to be $0.96 < A < 1$, which is an acceptable result. The smallest value of A was found for holo-Mb with $A = 0.9$. To illustrate the effect of large amplitudes of motion to the EISF we use a bimodal model to describe the holo-Mb data

$$A_0(q) = [\phi \cdot e^{-\langle x_1^2 \rangle q^2}(1 - \phi) \cdot e^{-\langle x_2^2 \rangle q^2}] \cdot (1 - p) + p \quad (9)$$

where we assume a value of $(\langle x_2^2 \rangle)^{1/2} = 2.5$ Å, which is in fact just the largest value of the displacement distribution function

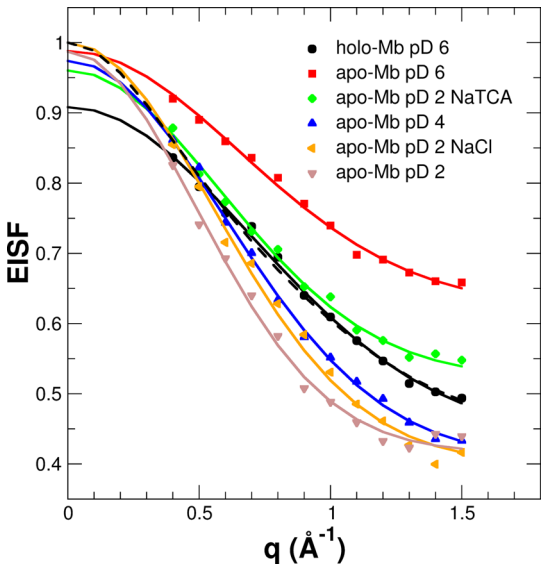

Figure 7. EISFs of the different samples. The solid lines are fits with eq 7. The dashed line is a fit of eq 8 to the data of holo-Mb.

shown by Doster and Settles.[44] The fit of the bimodal model is drawn in Figure 7 to show the behavior of the EISF at small q-values due to the hypothetical large amplitudes. We obtain $\phi = 0.24$, $\langle x_1^2 \rangle = 0.84$ Å^2, $p = 0.42$ from that fit. Allowing for even larger values of $(\langle x_2^2 \rangle)^{1/2}$ the $\langle x_1^2 \rangle$ then approaches the value of $\langle x^2 \rangle$ from eq 8. However, as experimental data are missing at $q < 0.4$ Å^{-1} we cannot reliably quantify the large amplitudes, if there should be any. Neutron backscattering experiments on hydrated powder samples reported acceptable results for $A \geq 0.8$ of the EISF.[45] In neutron backscattering experiments, such behavior of the EISF is a rather typical situation for protein dynamics at higher temperatures and it is usually ignored as only the initial slope is used for data analysis[46,47] corresponding to the model given in eq 8. The MSD due to vibrations was found to be uncorrelated with the secondary structure content and fluctuates around the average value of $\langle x_{vib}^2 \rangle = 0.14 \pm 0.05$ Å^2 for all samples.

The obtained MSDs and the fraction of immobile hydrogen atoms are shown in Figure 8 as a function of the measured α-helical secondary structure content in D_2O buffer. When the prefactor A in eq 8 is fixed at unity then the MSDs of native apo-Mb, the MG I1, the MG induced by NaCl, and the acid denatured state increase slightly by less than 0.1 Å^2. The MSD of holo-Mb is increased by 0.5 Å^2, and that of the MG I2, by 0.3 Å^2. However, keeping the prefactor A fixed at unity gives significantly worse fits especially to the holo-Mb data.

It is evident that the measured MSDs differ between the different structural conformations. In general, a larger amount of α-helical structure causes lower flexibility of the protein. The MGs show intermediate flexibility between the very flexible unfolded chain and the less flexible folded native apo- and holo-proteins. That behavior is similar to results regarding the dynamics of folded and intrinsically disordered proteins measured in solution.[48] In a previous study we investigated the dynamics of apo- and holo-Mb as hydrated powder samples using high-resolution neutron backscattering spectroscopy on the 0.1 ns time scale.[49] In that work we found apo-Mb to exhibit less flexibility compared to holo-Mb on the 0.1 ns time scale, while we observe apo-Mb to be more flexible than holo-Mb on the picosecond time scale in solution. The results

dx.doi.org/10.1021/jp509732q | J. Phys. Chem. B XXXX, XXX, XXX−XXX

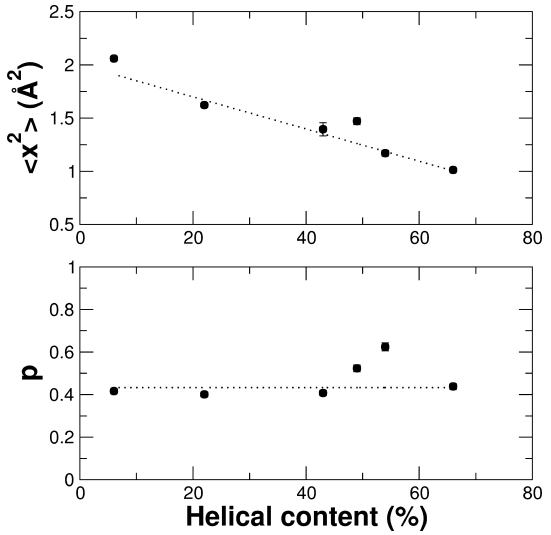

Figure 8. (A) MSD and (B) fraction of immobile hydrogens as a function of the measured secondary structure content.

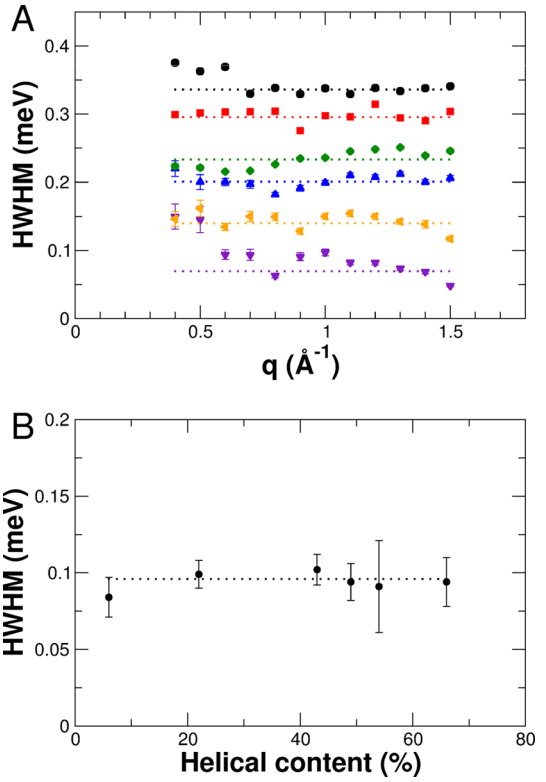

Figure 9. (A) Line widths of the quasielastic broadening. The dotted lines indicate the average values. For clarity the HWHM of the different samples are shifted consecutively by 0.05 meV. Symbols and colors are as in Figure 6. (B) Average values of the measured HWHM as a function of the measured secondary structure content of the proteins. The dotted line indicates the mean value of 0.096 meV.

demonstrate that the dynamics of two proteins can differ substantially between different hydration levels and time scales. Experiments concerning the dynamics of partially disordered and unfolded proteins should be performed in solution, where the protein can fully explore its conformational space without restrictions. Further high-resolution QENS experiments of the proteins in solution will shed more light on that aspect. The fraction of immobile hydrogens of the different structural conformations lies close to the average value of 0.43 with the exception of apo-Mb, which contains a larger amount of immobile hydrogens. The fraction of immobile hydrogens in folded globular proteins was attributed to slow moving amino acid side chains, which are located in the hydrophobic core of the protein.[11,12] Molecular dynamics simulations showed that the removal of the heme group allows water molecules to enter the heme pocket, which causes a redistribution of flexibility in the protein.[49] Active site residues in the heme cavity of apo-Mb were found to become more flexible, while the majority of the nonactive site residues showed reduced flexibility as compared to the holo-protein. Therefore, water molecules being present in the heme cavity of native apo-Mb appear to induce a larger fraction of slow moving side chains in the hydrophobic core. In the MGs and the acid denatured state the fraction of immobile hydrogens reaches the value of the native holo-Mb. That observation would indicate that in the MGs mostly slow moving amino acid side chains in the folded hydrophobic AGH nucleus, and in the acid denatured state residual helical elements in helices A and H and the local hydrophobic clusters in helices B and G, move slower and form the fraction of immobile hydrogens.

The half-widths $\Gamma(q)$ describing the quasielastic broadening are presented in Figure 9A for the different samples. Although the errors of $\Gamma(q)$ appear to be small, the intrinsic errors due to the strong D_2O background are certainly larger. Within the errors, the line widths were found to be independent of the scattering vector and could be approximated by a q-independent average value. The average values of the line widths are shown in Figure 9B as a function of the measured helical content.

The average $\langle\Gamma\rangle$ of the investigated samples fluctuate within the errors around the mean value of 0.096 meV corresponding to a correlation time of $1/\langle\Gamma\rangle$ = 6.9 ps.[24] The observed dynamics by QENS on the picosecond time scale was interpreted to arise from fast rotations and librations of the amino acid side chains around the consecutive C−C bonds.[11] Our results show that the correlation time of motions on the picosecond time scale is not significantly influenced by the structural composition of the apo- and holo-protein. The average value found in this work is in agreement with that of holo-Mb in solution as reported previously.[48]

3.3. Determination of Conformational Entropy by QENS. The difference in conformational entropy in proteins can be determined from QENS measurements as suggested by Receveur et al.[50] and Fitter[13] according to

$$\Delta S_{conf} = 3R \ln\left(\sqrt{\frac{\langle x_u^2\rangle}{\langle x_f^2\rangle}}\right) \quad (10)$$

where $\langle x_u^2\rangle$ and $\langle x_f^2\rangle$ are the MSDs of the unfolded state and the folded/partially folded conformation at the same temperature, and R = 8.3144 J/K/mol is the gas constant. In our work the acid denatured state is considered as a reference for the unfolded state. The determined values of ΔS_{conf} at 16 °C are shown in Figure 10 as a function of the measured α-helical content of the proteins.

We find an approximately linear increase of ΔS_{conf} with the helical structure content. The conformational entropy difference of the small Mb protein can be compared with previous results of larger multidomain proteins such as phosphoglycerate kinase (PGK)[50] or the heat stabile amylase from *B. licheniformis*

dx.doi.org/10.1021/jp509732q | J. Phys. Chem. B XXXX, XXX, XXX−XXX

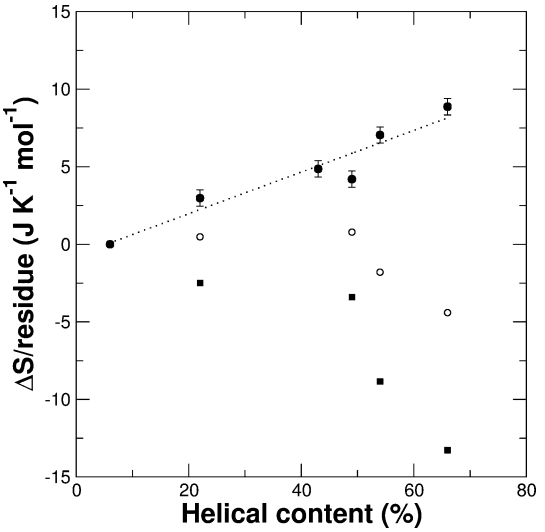

Figure 10. Entropy difference per residue of the different partially and fully folded conformations of apo-Mb and holo-Mb. The difference of conformational entropy ΔS_{conf} measured by neutron scattering (filled circles), the thermodynamic entropy difference $\Delta S = \Delta S_{conf} + \Delta S_{hydr}$ calculated with the Gibbs−Helmholtz equation with the known thermodynamic parameters (empty circles), and the difference $\Delta S_{hydr} = \Delta S - \Delta S_{conf}$ (filled squares) due to the entropy content of the hydration water and slow moving protein dynamics.

(BLA),[13] which have been investigated by QENS on the picosecond time scale. The melting temperature of PGK is 56 °C[51] being similar to the MGs and the native apo-Mb, while BLA has a high melting temperature of 103 °C,[13] which is larger than holo-Mb. The conformational entropy difference ΔS_{conf} of both proteins was found to be 4.7 J/K/mol for PGK at room temperature and 9.7 J/K/mol for BLA extrapolated to 16 °C. The conformational entropy difference of the MGs is similar to native PGK. Holo-Mb and BLA have a similar value of ΔS_{conf} although both proteins have different thermal stability. The comparison points out that the thermal stability of native proteins is reached by different mechanisms, where conformational entropy plays a specific role. In some cases partially folded MGs can even have a similar conformational entropy difference as native folded proteins.

The thermodynamic entropy difference $\Delta S = \Delta S_{conf} + \Delta S_{hydr}$ at 16 °C calculated with eq 6 with the thermodynamic parameters given in Table 1 is also shown in Figure 10. The thermodynamic entropy difference consists of the conformational entropy difference of the protein ΔS_{conf} and of the entropy difference of the hydration water ΔS_{hydr}. It is evident that the thermodynamic entropy difference of the MGs is only slightly larger than zero, while the folded native apo- and holo-proteins have negative values of ΔS. The physical reason for the difference between ΔS and ΔS_{conf} is the contribution of the hydration water to the thermodynamic measurements. The entropy content of the hydration water can be determined from the measured data by taking the difference $\Delta S_{hydr} = \Delta S - \Delta S_{conf}$. It is reasonable to assume that disordered and unfolded proteins explore a larger conformational space on longer time scales than fully folded native proteins. Hence, there is an additional contribution to the conformational entropy for the MGs and particularly for the fully folded proteins stemming from conformational motions on slower time scales, which cannot be detected by the neutron spectrometer used in this work. Thus, the real entropy difference due to the hydration water will have even smaller values than $\Delta S_{hydr} = \Delta S - \Delta S_{conf}$ especially for the folded native conformations. The values of ΔS_{hydr} shown in Figure 10, therefore, should be considered as an upper limit of the entropy difference related to the hydration water. Our results demonstrate that water molecules around the MGs are only slightly more dynamically disordered than in the unfolded state, whereas in the folded conformations the entropy content of the hydration water is significantly larger than in the MGs and in the unfolded state. Buried hydrophobic residues in the core of the protein are responsible for that effect, which become progressively more solvent exposed in the partially folded conformations than in the native states.

4. CONCLUSION

In this study we investigated the conformational fluctuations of apo- and holo-Mb in solution on the picosecond time scale. Different folded equilibrium states were prepared by modification of the solvent composition. The secondary structure content was found to have a significant impact on the measured MSDs, whereas the correlation times of the observed processes—attributed mainly to fast side chain rotations and librations—do not depend on the degree of folding. The direct comparison of the conformational entropy difference determined from the MSDs with the entropy difference obtained from thermodynamic measurements revealed the contribution of the hydration shell to the entropic stabilization of the proteins. Conformational motions in proteins extend over different time and length scales. In this work we focused on fast processes on the picosecond time scale mostly related to motions of amino acid side chains. A perspective for future work using neutron scattering could be to quantify the conformational entropy difference on the slower nanosecond time scale using high-resolution neutron time-of-flight and backscattering spectroscopy, whereas neutron spin−echo spectroscopy is the method of choice for the measurement of very slow dynamics up to several hundred nanoseconds. In this way one could disentangle, on which time scale the relevant conformational motions occur, which are responsible for protein folding.

■ ASSOCIATED CONTENT

Supporting Information

QENS spectra of apo-Mb in different folded states summed over the detector. This material is available free of charge via the Internet at http://pubs.acs.org.

■ AUTHOR INFORMATION

Corresponding Author

*E-mail: a.stadler@fz-juelich.de.

Notes

The authors declare no competing financial interest.

■ ACKNOWLEDGMENTS

A.S. would like to thank Prof. Dr. Dieter Richter for continuous support in his institute. This work is based on experiments performed at the Institut Laue-Langevin (ILL), Grenoble, France. We acknowledge the European Synchrotron Radiation Facility for provision of synchrotron radiation facilities, and we would like to thank Adam Round for assistance in using beamline BM29.

REFERENCES

(1) Dyson, H. J.; Wright, P. E. Unfolded Proteins and Protein Folding Studied by NMR. *Chem. Rev.* **2004**, *104*, 3607−3622.

(2) Dyson, H. J.; Wright, P. E. Equilibrium NMR Studies of Unfolded and Partially Folded Proteins. *Nat. Struct. Biol.* **1998**, *5*, 499−503.

(3) Eliezer, D.; Yao, J.; Dyson, H. J.; Wright, P. E. Structural and Dynamic Characterization of Partially Folded States of Apomyoglobin and Implications for Protein Folding. *Nat. Struct. Biol.* **1998**, *18*, 148−155.

(4) Loh, S. N.; Kay, M. S.; Baldwin, R. L. Structure and Stability of a Second Molten Globule Intermediate in the Apomyoglobin Folding Pathway. *Proc. Natl. Acad. Sci. U.S.A.* **1995**, *92*, 5446−5450.

(5) Jennings, P.; Wright, P. Formation of a Molten Globule Intermediate Early in the Kinetic Folding Pathway of Apomyoglobin. *Science (80-)* **1993**, *262*, 892−896.

(6) Jamin, M.; Baldwin, R. L. Two Forms of the pH 4 Folding Intermediate of Apomyoglobin. *J. Mol. Biol.* **1998**, *276*, 491−504.

(7) Ptitsyn, O. B. Molten Globule and Protein Folding. *Adv. Protein Chem.* **1995**, *47*, 83−229.

(8) Nick Pace, C.; Scholtz, J. M.; Grimsley, G. R. Forces Stabilizing Proteins. *FEBS Lett.* **2014**, *588*, 2177−2184.

(9) Ball, P. Water as an Active Constituent in Cell Biology. *Chem. Rev.* **2008**, *108*, 74−108.

(10) *Neutron Scattering in Biology - Techniques and Applications*; Fitter, J., Gutberlet, T., Katsaras, J., Eds.; Springer Berlin Heidelberg New York: Berlin, Heidelberg, 2006.

(11) Zanotti, J. M.; Bellissent-Funel, M. C.; Parello, J. Hydration-Coupled Dynamics in Proteins Studied by Neutron Scattering and NMR: The Case of the Typical EF-Hand Calcium-Binding Parvalbumin. *Biophys. J.* **1999**, *76*, 2390−2411.

(12) Stadler, A. M.; Garvey, C. J.; Embs, J. P.; Koza, M.; Unruh, T.; Artmann, G.; Zaccai, G. Picosecond Dynamics in Haemoglobin from Different Species: A Quasielastic Neutron Scattering Study. *Biochim. Biophys. Acta* **2014**, *1840*, 2989−2999.

(13) Fitter, J. A Measure of Conformational Entropy Change during Thermal Protein Unfolding Using Neutron Spectroscopy. *Biophys. J.* **2003**, *84*, 3924−3930.

(14) Covington, A. K.; Paabo, M.; Robinson, R. A.; Bates, R. G. Use of the Glass Electrode in Deuterium Oxide and the Relation between the Standardized pD (paD) Scale and the Operational pH in Heavy Water. *Anal. Chem.* **1968**, *40*, 700−706.

(15) Gasteiger, E.; Hoogland, C.; Gattiker, A.; Duvaud, S.; Wilkins, M. R.; Appel, R. D.; Bairoch, A. Protein Identification and Analysis Tools on the ExPASy Server. *The Proteomics Protocols Handbook*; Humana Press: 2005; pp 571−607.

(16) Antonini, E.; Brunori, M. *Hemoglobin and Myoglobin in Their Reactions with Ligands*; Neuberger, A., Tatum, E. L., Eds.; North-Holland Pub. Co.: Amsterdam, 1971.

(17) The ILL Yellow Book http://www.ill.eu/instruments-support/instruments-groups/yellowbook/ (accessed Sep 23, 2014).

(18) LAMP, the Large Array Manipulation Program http://www.ill.eu/data_treat/lamp/the-lamp-book/.

(19) Svergun, D. I.; Koch, M. H. J. Small-Angle Scattering Studies of Biological Macromolecules in Solution. *Rep. Prog. Phys.* **2003**, *66*, 1735−1782.

(20) Pernot, P.; Round, A.; Barrett, R.; De Maria Antolinos, A.; Gobbo, A.; Gordon, E.; Huet, J.; Kieffer, J.; Lentini, M.; Mattenet, M.; et al. Upgraded ESRF BM29 Beamline for SAXS on Macromolecules in Solution. *J. Synchrotron Radiat.* **2013**, *20*, 660−664.

(21) Svergun, D. I. Determination of the Regularization Parameter in Indirect-Transform Methods Using Perceptual Criteria. *J. Appl. Crystallogr.* **1992**, *25*, 495−503.

(22) Sreerama, N.; Woody, R. W. Estimation of Protein Secondary Structure from Circular Dichroism Spectra: Comparison of CONTIN, SELCON, and CDSSTR Methods with an Expanded Reference Set. *Anal. Biochem.* **2000**, *287*, 252−260.

(23) Provencher, S. W. CONTIN: A General Purpose Constrained Regularization Program for Inverting Noisy Linear Algebraic and Integral Equations. *Comput. Phys. Commun.* **1982**, *27*, 229−242.

(24) Bée, M. *Quasielastic Neutron Scattering: Principles and Applications in Solid State Chemistry, Biology, and Materials Science*; Adam Hilger: Bristol, Philadelphia, 1988.

(25) Parak, F. G. Physical Aspects of Protein Dynamics. *Rep. Prog. Phys.* **2003**, *66*, 103−129.

(26) Hersleth, H.-P.; Uchida, T.; Røhr, A. K.; Teschner, T.; Schünemann, V.; Kitagawa, T.; Trautwein, A. X.; Görbitz, C. H.; Andersson, K. K. Crystallographic and Spectroscopic Studies of Peroxide-Derived Myoglobin Compound II and Occurrence of Protonated FeIV O. *J. Biol. Chem.* **2007**, *282*, 23372−23386.

(27) Eliezer, D.; Wright, P. E. Is Apomyoglobin a Molten Globule? Structural Characterization by NMR. *J. Mol. Biol.* **1996**, *263*, 531−538.

(28) Hughson, F.; Wright, P.; Baldwin, R. Structural Characterization of a Partly Folded Apomyoglobin Intermediate. *Science (80-)* **1990**, *249*, 1544−1548.

(29) Eliezer, D.; Chung, J.; Dyson, H. J.; Wright, P. E. Native and Non-Native Secondary Structure and Dynamics in the pH 4 Intermediate of Apomyoglobin. *Biochemistry* **2000**, *39*, 2894−2901.

(30) Yao, J.; Chung, J.; Eliezer, D.; Wright, P. E.; Dyson, H. J. NMR Structural and Dynamic Characterization of the Acid-Unfolded State of Apomyoglobin Provides Insights into the Early Events in Protein Folding. *Biochemistry* **2001**, *40*, 3561−3571.

(31) Nishii, I.; Kataoka, M.; Goto, Y. Thermodynamic Stability of the Molten Globule States of Apomyoglobin. *J. Mol. Biol.* **1995**, *250*, 223−238.

(32) Kataoka, M.; Nishii, I.; Fujisawa, T.; Ueki, T.; Tokunaga, F.; Goto, Y. Structural Characterization of the Molten Globule and Native States of Apomyoglobin by Solution X-ray Scattering. *J. Mol. Biol.* **1995**, *249*, 215−228.

(33) Nishii, I.; Kataoka, M.; Tokunaga, F.; Goto, Y. Cold Denaturation of the Molten Globule States of Apomyoglobin and a Profile for Protein Folding. *Biochemistry* **1994**, *33*, 4903−4909.

(34) Privalov, P. L.; Khechinashvili, N. N. A Thermodynamic Approach to the Problem of Stabilization of Globular Protein Structure: A Calorimetric Study. *J. Mol. Biol.* **1974**, *86*, 665−684.

(35) Griko, Y. V.; Privalov, P. L.; Venyaminov, S. Y.; Kutyshenko, V. P. Thermodynamic Study of the Apomyoglobin Structure. *J. Mol. Biol.* **1988**, *202*, 127−138.

(36) Johansen, D.; Jeffries, C. M. J.; Hammouda, B.; Trewhella, J.; Goldenberg, D. P. Effects of Macromolecular Crowding on an Intrinsically Disordered Protein Characterized by Small-Angle Neutron Scattering with Contrast Matching. *Biophys. J.* **2011**, *100*, 1120−1128.

(37) Soranno, A.; Koenig, I.; Borgia, M. B.; Hofmann, H.; Zosel, F.; Nettels, D.; Schuler, B. Single-Molecule Spectroscopy Reveals Polymer Effects of Disordered Proteins in Crowded Environments. *Proc. Natl. Acad. Sci. U.S.A.* **2014**, *111*, 4874−4879.

(38) Sasahara, K.; McPhie, P.; Minton, A. P. Effect of Dextran on Protein Stability and Conformation Attributed to Macromolecular Crowding. *J. Mol. Biol.* **2003**, *326*, 1227−1237.

(39) Tokuriki, N.; Kinjo, M.; Negi, S.; Hoshino, M.; Goto, Y.; Urabe, I.; Yomo, T. Protein Folding by the Effects of Macromolecular Crowding. *Protein Sci.* **2004**, *13*, 125−133.

(40) Stadler, A. M.; Stingaciu, L.; Radulescu, A.; Holderer, O.; Monkenbusch, M.; Biehl, R.; Richter, D. Internal Nanosecond Dynamics in the Intrinsically Disordered Myelin Basic Protein. *J. Am. Chem. Soc.* **2014**, *136*, 6987−6994.

(41) Akaike, H. A New Look at the Statistical Model Identification. *IEEE Trans. Automat. Contr.* **1974**, *19*, 716−723.

(42) Zorn, R. Multiple Scattering Correction of Neutron Scattering Elastic Scans. *Nucl. Instruments Methods Phys. Res. Sect. A Accel. Spectrometers, Detect. Assoc. Equip.* **2007**, *572*, 874−881.

(43) Zorn, R. On the Evaluation of Neutron Scattering Elastic Scan Data. *Nucl. Instruments Methods Phys. Res. Sect. A Accel. Spectrometers, Detect. Assoc. Equip.* **2009**, *603*, 439−445.

(44) Doster, W.; Settles, M. Protein-Water Displacement Distributions. *Biochim. Biophys. Acta* **2005**, *1749*, 173−186.
(45) Peters, J.; Kneller, G. R. Motional Heterogeneity in Human Acetylcholinesterase Revealed by a Non-Gaussian Model for Elastic Incoherent Neutron Scattering. *J. Chem. Phys.* **2013**, *139*, 165102.
(46) Trapp, M.; Trovaslet, M.; Nachon, F.; Koza, M. M.; van Eijck, L.; Hill, F.; Weik, M.; Masson, P.; Tehei, M.; Peters, J. Energy Landscapes of Human Acetylcholinesterase and Its Huperzine A-Inhibited Counterpart. *J. Phys. Chem. B* **2012**, *116*, 14744−14753.
(47) Stadler, A. M.; Garvey, C. J.; Bocahut, A.; Sacquin-Mora, S.; Digel, I.; Schneider, G. J.; Natali, F.; Artmann, G. M.; Zaccai, G. Thermal Fluctuations of Haemoglobin from Different Species: Adaptation to Temperature via Conformational Dynamics. *J. R. Soc. Interface* **2012**, *9*, 2845−2855.
(48) Gaspar, A. M.; Appavou, M.-S.; Busch, S.; Unruh, T.; Doster, W. Dynamics of Well-Folded and Natively Disordered Proteins in Solution: A Time-of-Flight Neutron Scattering Study. *Eur. Biophys. J.* **2008**, *37*, 573−582.
(49) Stadler, A. M.; Pellegrini, E.; Johnson, M.; Fitter, J.; Zaccai, G. Dynamics-Stability Relationships in Apo- and Holomyoglobin: A Combined Neutron Scattering and Molecular Dynamics Simulations Study. *Biophys. J.* **2012**, *102*, 351−359.
(50) Receveur, V.; Calmettes, P.; Smith, J. C.; Desmadril, M.; Coddens, G.; Durand, D. Picosecond Dynamical Changes on Denaturation of Yeast Phosphoglycerate Kinase Revealed by Quasielastic Neutron Scattering. *Proteins* **1997**, *28*, 380−387.
(51) Hu, C. Q.; Sturtevant, J. M. Thermodynamic Study of Yeast Phosphoglycerate Kinase. *Biochemistry* **1987**, *26*, 178−182.